Experimental Mechanics (2019) 59:279–293
https://doi.org/10.1007/s11340-018-0423-2

Material Flaw Populations and Component Strength Distributions in the Context of the Weibull Function

R.F. Cook[1] · F.W. DelRio[2]

Received: 21 February 2018 / Accepted: 25 July 2018 / Published online: 14 August 2018

Abstract
A clear relationship between the population of brittle-fracture controlling flaws generated in a manufactured material and the distribution of strengths in a group of selected components is established. Assumptions regarding the strength-flaw size relationship, the volume of the components, and the number in the group, are clarified and the contracting effects of component volume and truncating effects of group number on component strength empirical distribution functions highlighted. A simple analytical example is used to demonstrate the forward prediction of population → distribution and the more important reverse procedure of empirical strength distribution → underlying flaw population. Three experimental examples are given of the application of the relationships to state-of-the-art micro- and nano-scale strength distributions to experimentally determine flaw populations: two on etched microelectromechanical systems (MEMS) structures and one on native and oxidized silicon nanowires. In all examples, the minimum threshold strength and conjugate maximum flaw size are very well estimated and the complete flaw population, including the minimum flaw size, are very poorly estimated, although etching, bimodal, and oxidation effects were clearly discernible. The results suggest that the best use of strength distribution information for MEMS manufacturers and designers might be in estimation of the strength threshold.

Keywords Distribution · Fracture · Probability · Flaw · Strength · Weibull

Introduction

Manufacturing processes typically produce large numbers of components that comprise the entire volume of manufactured material. For components that are intended to be primarily structural (i.e., load bearing) attention focuses on the population of strength-limiting defects or flaws generated by a particular manufacturing process and distributed throughout the material volume. Such flaws control the strength of the material local to the flaw and manufacturing processes for structural components are optimized to maximize the strength (subject to constraints of cost, timeliness, aesthetics, etc. [1]). Under usual circumstances, the flaws are much smaller than the volume of manufactured material and the components, e.g., fragmentation cracks in glazed pottery, grinding striations in machined material, grain-boundary grooves in etched microelectromechanical systems (MEMS), and atomic-scale defects in vapor-phase grown nanostructures (although there are exceptions, e.g., the macroscopic crack in the Liberty Bell casting). A component formed from the manufactured material will thus likely contain a number of flaws sampled from the population. A simple method of interrogating the effects of processing changes is thus to measure the strength of a component and infer the strength-controlling flaw size from a known or assumed strength-flaw size relationship. A key question is thus "What can strength distribution measurements on a selected small group of manufactured components say about the large population of flaws produced in materials by a manufacturing process?"

The above question has particular relevance for designers of small-scale components as manufacturing enters the micro- and nano-scale. Manufacturing processes determine entire populations of flaws but must be optimized by constrained measurements on subsets of flaws within groups of such components: (1) Establishing statistically-meaningful strength distributions is difficult on small-scale components, although great progress has been made using specialized test structures

✉ R. F. Cook
robert.cook@nist.gov

[1] Materials Measurement Science Division, National Institute of Standards and Technology, Gaithersburg, MD 20899, USA

[2] Applied Chemicals and Materials Division, National Institute of Standards and Technology, Boulder, CO 80305, USA

[2–7]; (2) Interpreting strengths in terms of small-scale flaw failure mechanisms is often ambiguous, e.g., the difference between a crack, a notch, and a contact impression at the nano-scale is not always obvious from a strength measurement [8]; and, (3) The group of small-scale test components is often very small relative to the number of manufactured devices, e.g., tests of hundreds of MEMS sensors are dwarfed by the hundreds of millions that are installed in automobiles each year, comprising the $10B market [9]. Hence, micro- and nano-scale device manufacturers must optimize materials processing using strength-measurement data as a probe of flaw populations under conditions in which the data are difficult to obtain, interpreting the data can be ambiguous, and, nevertheless, the data are then highly leveraged. An answer beyond "small strengths imply large flaw sizes, and *vice versa*" is required to optimize micro- and nano-scale manufacturing in a cost-effective manner.

An answer to the question is given here by establishing clear mathematical linkages between the parameters describing the flaw population and those describing the strength distribution of components. The linkages between flaw population and strength distribution are first established in a "forward" direction, by assuming a flaw population in a brittle material and then developing the framework to arrive at the resulting group fracture-strength distribution. A simple, symmetric flaw population is assumed here for demonstration. The importance of upper bounds in flaw populations [10] in determining lower-bound strength thresholds and of component scale and group size [11] in determining upper-bound strength limits is made clear, extending previous work [12–15]. The established linkages are then used in a "reverse" (or "inverse" [16]) direction, by fitting a commonly-used strength distribution function—the Weibull function—to the quadratically-generated group of components and examining the implications for the inferred underlying flaw population. Three small-scale experimental example applications of gradually increasing complexity are then introduced to demonstrate the use of the linkages to determine underlying flaw populations from strength tests, allowing direct comparison with independent measurements: two on micro-scale silicon (Si) MEMS structures and one on silicon nanowires (SiNWs). A discussion considers the merits of strength testing and previous work in this area.

Fracture Probability Analysis

Material Flaw Population

Analysis begins by considering a manufacturing process that generates a large population of (brittle fracture) strength-controlling features in a total volume Ω of manufactured material, Fig. 1(a). The features have an average density λ (number/volume) in the material. The feature sizes, c, vary from feature to feature and the primary intention is that c is a physical length dimension, say an etch-pit depth or a crack length, that determines the local strength of the material. c is thus referred to as a "flaw size." The reciprocal of λ defines the volume $\Delta V = 1/\lambda$. ΔV is chosen to be sufficiently small (or λ sufficiently large) such that each volume ΔV contains exactly one feature arising from the manufacturing process and ΔV thus defines a fundamental volume element, Fig. 1(b). (An obvious physical dimension limitation is that, on average, $c \le \Delta V^{1/3}$. c could also be a dimensionless geometrical characteristic, say an etch-pit aspect ratio, or a manufacturing parameter of a non-length dimension, say an etching time or an abrasive load.) The population of elements ($\Omega/\Delta V$) is sufficiently large that the flaw sizes may be treated as a continuum and thus there exists a probability density function (pdf), $f(c)$, describing the flaw sizes over the domain $c_{\min} \le c \le c_{\max}$. $c_{\min}$ and $c_{\max}$ are the minimum and maximum flaw sizes in the population, respectively. $f(c)$ can be considered as the fundamental property of the population and has finite or bounded support between $c_{\min}$ and $c_{\max}$. A simple, symmetric form for $f(c)$ to be used here as an example is the quadratic pdf

$$f(c) = \begin{cases} 0, 0 \le c \le c_{\min} \\ \dfrac{6(c-c_{\min})(c_{\max}-c)}{(c_{\max}-c_{\min})^3}, c_{\min} \le c \le c_{\max} \\ 0, c > c_{\max} \end{cases} \quad (1)$$

shown in Fig. 2(a) using $c_{\min} = 1$ μm and $c_{\max} = 16$ μm. The early "forward" analyses were also carried out using simple, but unbounded, unimodal $f(c)$ expressions, [12, 13], based on surface indentation tests [17–21] that determine $\lambda(c)$. These tests also suggest that $c << \Delta V^{1/3}$, i.e., that defects are "rare" or "dilute", an assumption often made in early analyses [e.g., 22] and more recent simulations [e.g., 23, 24] and which shall be seen later to be important for the current analysis. Experimental determination of $f(c)$ may also be used directly [25].

Integration of the pdf gives the cumulative distribution function (cdf), $F(c)$ [26],

$$F(c) = \int_0^c f\left(c'\right) \mathrm{d}c'. \quad (2)$$

$F(c)$ gives the proportion of the population of elements with flaw sizes smaller than c and is thus the probability that an element selected at random from the population will have a flaw size smaller than c. Note that integration outside the region of support is zero,

$$\int_0^{c_{\min}} f\left(c'\right) \mathrm{d}c' = \int_{c_{\max}}^{\infty} f\left(c'\right) \mathrm{d}c' = 0$$

and that normalization of the pdf requires

$$\int_{c_{\min}}^{c_{\max}} f\left(c'\right) \mathrm{d}c' = 1.$$

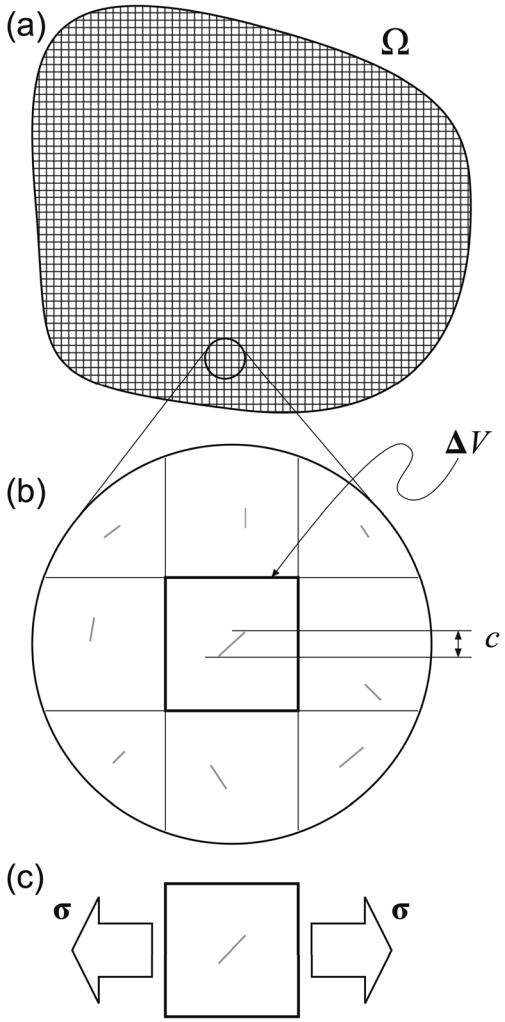

Fig. 1 **(a)** Schematic diagram of a large volume of manufactured material containing a population of fundamental volume elements. **(b)** Each fundamental element has volume ΔV and contains exactly one strength-controlling flaw of size c, forming a material population of flaw sizes. **(c)** The brittle fracture strength of each fundamental volume element is σ, forming a material population of strengths

The cdf $F(c)$ thus increases from 0 to 1 over the region of support $c_{\min} \le c \le c_{\max}$. The example quadratic pdf in equation (1) above meets the normalization requirement and thus the resulting cdf is, Fig. 2(b),

$$F(c) = \begin{cases} 0, 0 \le c \le c_{\min} \\ 3\left(\frac{c-c_{\min}}{c_{\max}-c_{\min}}\right)^2 - 2\left(\frac{c-c_{\min}}{c_{\max}-c_{\min}}\right)^3, c_{\min} \le c \le c_{\max} \\ 1, c > c_{\max} \end{cases} \tag{3}$$

The pdf and cdf given above describe the population of flaw sizes. To begin to make connection with the distribution of component strengths, a relationship between element strength and flaw size is required. One of the simplest is the Griffith relation [27].

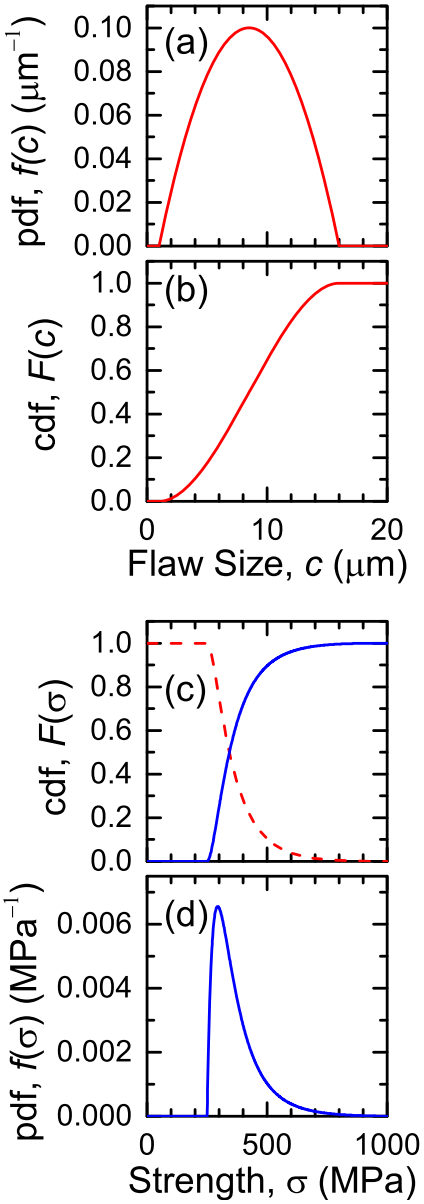

Fig. 2 **(a)** The flaw-size probability density function (pdf), $f(c)$, for the example quadratic material population of flaws, equation (1). **(b)** The flaw-size cumulative distribution function (cdf), $F(c)$, for the quadratic material population of flaws, equation (3). **(c)** The strength complementary cumulative distribution function (ccdf), $\overline{F}(\sigma)$ (dashed line), equation (7), and the strength cdf, $F(\sigma)$ (solid line), for the quadratic material population of flaws. **(d)** The strength pdf, $f(\sigma)$, for the quadratic material population of flaws, equation (9)

$$\sigma = Bc^{-1/2}, \tag{4}$$

where σ is the strength, Fig. 1(c), of an element containing flaw size c, here taken as the length of a crack. B is a constant with dimensions of [strength][length]$^{1/2}$ involving the element toughness, set by the material, and the flaw geometry and residual stress state, set by the manufacturing process. (A typical value for $B = 1$ MPa m$^{1/2}$, used in the example figures,

such that a flaw size of $c = 1$ μm corresponds to a strength of $\sigma = 1$ GPa [27].) More complicated relations than the above are possible [e.g., 25], but all retain an inverse relationship between strength and flaw size. Setting

$$\sigma_u = Bc_{min}^{-1/2} \tag{5a}$$

gives the upper limit to the element strengths, σ_u, corresponding to the minimum in the population flaw-size distribution. Similarly,

$$\sigma_{th} = Bc_{max}^{-1/2} \tag{5b}$$

gives the lower limit to the element strengths, σ_{th}, corresponding to the maximum in the population flaw-size distribution. The lower bound to the strength, σ_{th}, is critical for design and is known as the "threshold strength".

Direct substitution of the above strength relations, equations (4) and (5), into the flaw-size cdf, equation (2), gives the complementary cumulative distribution function, ccdf, or *exceedance*, $\overline{F}(\sigma)$, for the element strength population related to the cdf by

$$\overline{F}(\sigma) = 1 - F(\sigma). \tag{6}$$

(The "ccdf" or "exceedance" are not terms particular to strengths or flaws. $\overline{F}(x)$ is also commonly known as a "tail distribution" for a general variable x, or as the reliability or survival function, $\overline{F}(t)$, sometimes denoted $R(t)$ or $S(t)$, in lifetime analyses [26, 28, 29]). The cdf $F(c)$ gives the probability that an element selected from the population has a flaw size smaller than c. The ccdf $\overline{F}(\sigma)$ gives the probability that an element selected from the population has a strength *greater* than σ (or *exceeds* σ). Just as the cdf $F(c)$ ranges between 0 and 1 over the region of support $c_{min} \le c \le c_{max}$ for the population of flaws, the ccdf $\overline{F}(\sigma)$ ranges between 1 and 0 over the conjugate region of support $\sigma_{th} \le \sigma \le \sigma_u$ for the population of strengths. The inverse relationship between σ and c underpins these relationships. $\overline{F}(\sigma)$ for the simple quadratic population is given by, Fig. 2(c),

$$\overline{F}(\sigma) = \begin{cases} 1, 0 \le \sigma \le \sigma_{th} \\ 3\left(\dfrac{\sigma^{-2}-\sigma_u^{-2}}{\sigma_{th}^{-2}-\sigma_u^{-2}}\right)^2 - 2\left(\dfrac{\sigma^{-2}-\sigma_u^{-2}}{\sigma_{th}^{-2}-\sigma_u^{-2}}\right)^3, \sigma_{th} \le \sigma \le \sigma_u \\ 0, \sigma > \sigma_u \end{cases} \tag{7}$$

The population exceedance is of little direct interest as the strengths of individual fundamental elements are rarely measured singly, Fig. 1(c), but $\overline{F}(\sigma)$ is of crucial importance in developing the strength distributions of groups of multi-element components (as shown in the next section). Similarly, the population cdf for strength, $F(\sigma)$, Fig. 2(c), is only of interest as a limiting function for comparison with distributions of components [30, 31]. However, the population pdf for strength, $f(\sigma)$, is often of interest in cases in which the relationship between strength and flaw size is unknown. Noting that the integral of equation (2) applies to strength as

$$F(\sigma) = \int_0^\sigma f\left(\sigma'\right) \mathrm{d}\sigma'$$

the derivative form is

$$f(\sigma) = \frac{\mathrm{d}F(\sigma)}{\mathrm{d}\sigma}. \tag{8}$$

$f(\sigma)$ for the simple quadratic population is thus given by, Fig. 2(d),

$$f(\sigma) = \begin{cases} 1, 0 \le \sigma \le \sigma_{th} \\ 12\dfrac{\left(\sigma^{-2}-\sigma_u^{-2}\right)\left(\sigma_{th}^{-2}-\sigma_u^{-2}\right)}{\left[\sigma\left(\sigma_{th}^{-2}-\sigma_u^{-2}\right)\right]^3}, \sigma_{th} \le \sigma \le \sigma_u \\ 0, \sigma > \sigma_u \end{cases} \tag{9}$$

where $\sigma_{min} = 250$ MPa and $\sigma_{max} = 1000$ MPa using equation (5) and $B = 1$ MPa m$^{1/2}$. There are several points to note from Eqs. (1) to (9) and Fig. 2. First, symmetric forms of flaw-size pdf and cdf give rise to asymmetric forms of strength pdf and cdf. Second, the analysis is quite straightforward, but does require recognition that the inverse relationship between σ and c leads to the identification of the cdf $F(c)$ with the ccdf $\overline{F}(\sigma)$, an identification made in many earlier works, although not in the form above [e.g., 12,13,15,22,25,32–35] (strictly, all that is required for this identification is that $\mathrm{d}\sigma/\mathrm{d}c < 0$). Third, a simple expression for the fundamental flaw-size pdf $f(c)$, equation (1), led to a much more complicated expression for the resulting strength ccdf $\overline{F}(\sigma)$, equation (7). The implication from these three points is that it would not be obvious what the mathematical description an unknown pdf or cdf describing fracture would take given the form of a related pdf or cdf.

Component Strength Distribution

$F(c)$ is the probability that a single fundamental element selected randomly from the population will have a flaw size smaller than c. If it is assumed that the elements (and thus their flaws) are independent, the probability $F_{2\Delta V}(c)$ that two elements selected from the population will both have flaw sizes smaller than c is given by the product of their probabilities taken singly [5].

$$F_{2\Delta V}(c) = F(c) \cdot F(c).$$

Thus, the probability $F_{k\Delta V}(c)$ that k elements selected from the population will all have feature sizes smaller than c is

$$F_{k\Delta V}(c) = F_V(c) = F(c)^k$$

If the k elements form a single component of volume $V = k\Delta V$, $F_V(c)$ is the probability that the component contains only flaws smaller than c or the probability that c is the largest flaw size in

the component. If a group of many similarly-formed components of volume V is assembled, $F_V(c)$ is the proportion of components within the group that contain only flaws smaller than c or in which c is the largest flaw.

Similarly, if k elements are selected from the population and are independent, the probability that all k elements have a strength greater than σ is

$$\overline{F}_{k\Delta V}(\sigma) = \overline{F}_V(\sigma) = \overline{F}(\sigma)^k. \tag{10}$$

If the k elements form a single component of volume V as above, $\overline{F}_V(\sigma)$ is the probability that the component has a strength greater than σ. If a group of many similarly-formed components, all of volume V, is assembled, Fig. 3, $\overline{F}_V(\sigma)$ is the proportion of components within the group that have a strength greater than σ. The *group* exceedance resulting from the above quadratic *population* exceedance, equation (7), is thus (for the number of components in the group, N, very large, the group exceedance can be approximated as a continuum distribution)

$$\overline{F}_V(\sigma) = \begin{cases} 1, 0 \le \sigma \le \sigma_{\text{th}} \\ \left[3\left(\dfrac{\sigma^{-2}-\sigma_{\text{u}}^{-2}}{\sigma_{\text{th}}^{-2}-\sigma_{\text{u}}^{-2}}\right)^2 - 2\left(\dfrac{\sigma^{-2}-\sigma_{\text{u}}^{-2}}{\sigma_{\text{th}}^{-2}-\sigma_{\text{u}}^{-2}}\right)^3 \right]^k, \sigma_{\text{th}} \le \sigma \le \sigma_{\text{u}} \\ 0, \sigma > \sigma_{\text{u}} \end{cases} \tag{11}$$

The region of support and range of $\overline{F}_V(\sigma)$ are identical to those of $\overline{F}(\sigma)$. The generation of $\overline{F}_V(\sigma)$ from $\overline{F}(\sigma)$ is based on the independence of the fundamental volume elements and is consistent with "weakest-link" arguments, in which a chain (component) is only as strong as its weakest link (element) (if the links are independent, the strength of the chain is not altered by the presence or absence of links that are stronger than the weakest link.) Independence and weakest link ideas were used by Weibull and Epstein in early considerations of strength variability [36–39], consistent with dilute or "isolated" populations of flaws (i.e., $c << \Delta V^{1/3}$) and the absence of "non-local" effects in brittle fracture strengths [32, 40, 41]. The cdf of a strength distribution is complementary to the ccdf, and thus the cdf for the group of component strengths, $F_V(\sigma)$, is given by

$$\begin{aligned} F_V(\sigma) &= 1 - \overline{F}_V(\sigma) \\ &= 1 - \overline{F}(\sigma)^k \end{aligned} \tag{12}$$

$F_V(\sigma)$ is the probability that a component of volume V has a strength *less* than σ, i.e., the component will *fail* if exposed to a stress of σ. If a group of many similarly-formed components is assembled, $F_V(\sigma)$ is the proportion of components within the group that will fail if exposed to a stress of σ. $F_V(\sigma)$ component strength cdf curves for values of k = 2, 5, and 50 for the simple quadratic flaw pdf are shown in Fig. 4, along with the population strength cdf $F(\sigma)$. The region of support and range of $F_V(\sigma)$ are identical to those of $F(\sigma)$ but the function is much more strongly varying near σ_{th} (independent of the mathematical form of $\overline{F}(\sigma)$), approaching 1 more rapidly as k increases.

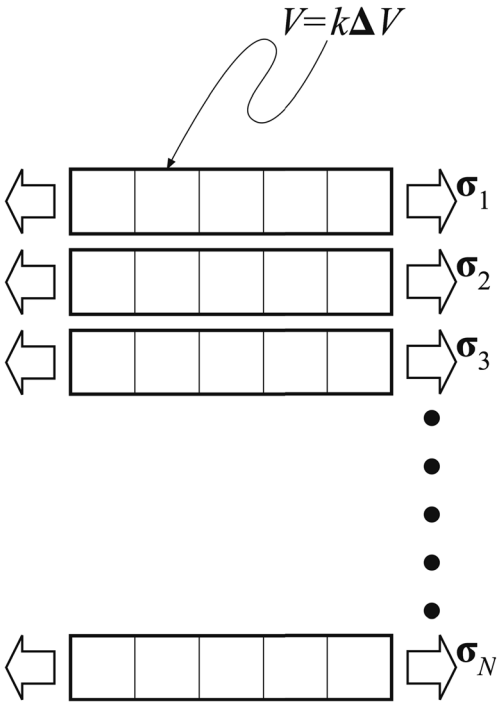

Fig. 3 Schematic diagram of a group of N components, each of volume V consisting of k fundamental volumes ΔV. Each component has a strength σ_i that can be ranked from 1 to N in an empirical distribution function

The group of components in Fig. 4 is considered sufficiently large that the component strengths may be treated as a continuum and the cdf $F_V(\sigma)$ may thus be treated as continuous. This is not true generally but provides a convenient reference. As noted above, the domain of variation of component strengths is much narrower than the population of element strengths set by the population of flaw sizes; a result noted earlier [10]. That is, the transition from near certain survival, $F_V(\sigma) \approx 0$ to near certain failure, $F_V(\sigma) \approx 1$ occurs over a much smaller stress range for components than the population. At small strengths, both the component and population strength distributions are terminated by the strength threshold associated with the maximum flaw size. As the strength and probability of failure increases however, the component strength distribution approaches near certainty of failure at strength levels much less than those set by the population, as a consequence of combining many fundamental elements into a single component (Fig. 3). This narrowing tendency increases as the component size increases, quantified by k (k need not be an integer, except for chains). The average strength within a group of components decreases as the component size increases. The limit of both these trends is that k equals the

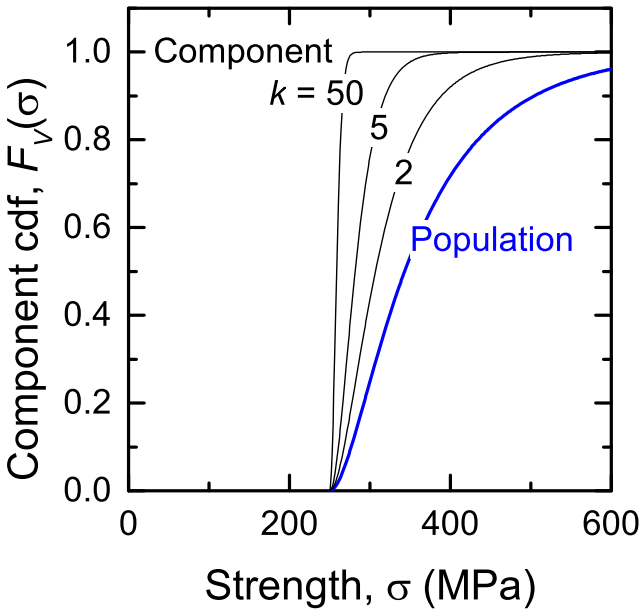

Fig. 4 Plot of the strength cumulative distribution function (cdf), $F_V(\sigma)$, for large groups of components of different volumes $V = k\Delta V$ (Eqs. (11) and (12)) for the quadratic material population of flaws. The cdf of the population (equivalent to $k = 1$) is shown as the bold line (Fig. 2(c)). As the component size increases (k increases), the group strength cdf is contracted and decreases away from the population cdf towards the limiting threshold

population; the single limiting component contains all the flaws from the population, including the largest flaw, and thus exhibits the threshold strength. In practice, k need only be > ≈100 for $F_V(\sigma)$ to appear as a near step-function. Good examples of contraction with increasing k are shown by experiments with MEMS samples [7] and paper strips of increasing length [42].

Empirical Distribution Function

As the number of components within a group is finite, σ and F_V take only discrete values. However, it is possible to estimate the continuous cdf and pdf of a material population by a discrete function of the measured or calculated strengths of a group of components. This function is termed the "empirical distribution function" and is such that at any specified measured strength the value of the function is the fraction of observations within the group that has strengths less than or equal to the specified strength. Operationally, for a group containing N components, the component strengths are part of the sequence σ_i, in which the index i (or rank) runs from 1 to N. The sequence is ordered, such that σ_1 is the smallest measured strength and σ_N is the largest. The quantity $P_i = (i - 0.5)/N$ is formed for each strength; P_1 is the smallest number (near zero) and P_N is the largest (near 1). If a strength σ_i is selected from the ordered sequence, the conjugate number P_i gives the proportion of N for which the measured strengths are less than σ_i: $P_i(\sigma_i)$ thus provides a statistical measure of $F_V(\sigma)$. An empirical distribution function can obviously be generated for experimental or analytical groups of strengths.

The empirical distribution functions, $P_i(\sigma_i)$, for component strengths within groups of various numbers, $N = 10$, 30, and 100, are shown in Fig. 5. The discrete component strengths were determined from the simple quadratic population flaw-size pdf using a component size of $k = 5$ and are shown as the open symbols. The population strength cdf, $F(\sigma)$, is shown as the solid line. The domains of strengths within the discrete empirical distribution functions are shifted to smaller strengths than the continuous population of strengths set by the population of elements, and are much narrower, consistent with the continuous $F_V(\sigma)$ curves shown above. At small strengths, the component empirical distribution functions are terminated by the strength threshold associated with the maximum flaw size within the population. At large strengths, the component empirical distribution functions are terminated by the strongest component within the group. The strength of this strongest component, and the average strength within a group, increased with the number of components within the group, but both fell well below the values set by the population. The limit of these trends is that as N/k approaches its maximum value (assuming sampling without replacement from the population of elements), the group of components contains all the flaws from the population, including the largest and smallest flaws, and thus the empirical distribution function will approach the population cdf.

Weibull Distribution Function

The above development highlighted the increasing analytical complexity in proceeding from a simple population flaw-size pdf (a quadratic) to a more complicated group strength cdf. As it is fundamental to consider a population of flaws from a theoretical point of view, it makes sense to proceed analytically in this "forward" direction. However, it is far easier and more common to consider a group of components from the experimental point of view of the empirical distribution of strengths. Hence, it makes sense to fit a simple cdf to the empirical distribution function and then proceed in the "reverse" direction to a (potentially) more complicated population flaw-size pdf. Hence, many groups of components are described by a (simple) stretched exponential cdf, often known as a Weibull [37] (or Fréchet or Rosin-Rammler [43, 44]) distribution function

$$F_{\text{group}}(\sigma) = 1 - \exp\left[-\left(\frac{\sigma - \sigma_{\text{th}}}{\sigma_\theta}\right)^m\right] \tag{13}$$

over the (unbounded) region of support $\sigma \geq \sigma_{\text{th}}$ ($m = 1$ corresponds to the exponential distribution [28, 43], $m = 2$ corresponds to the Rayleigh distribution [43]). The subscript

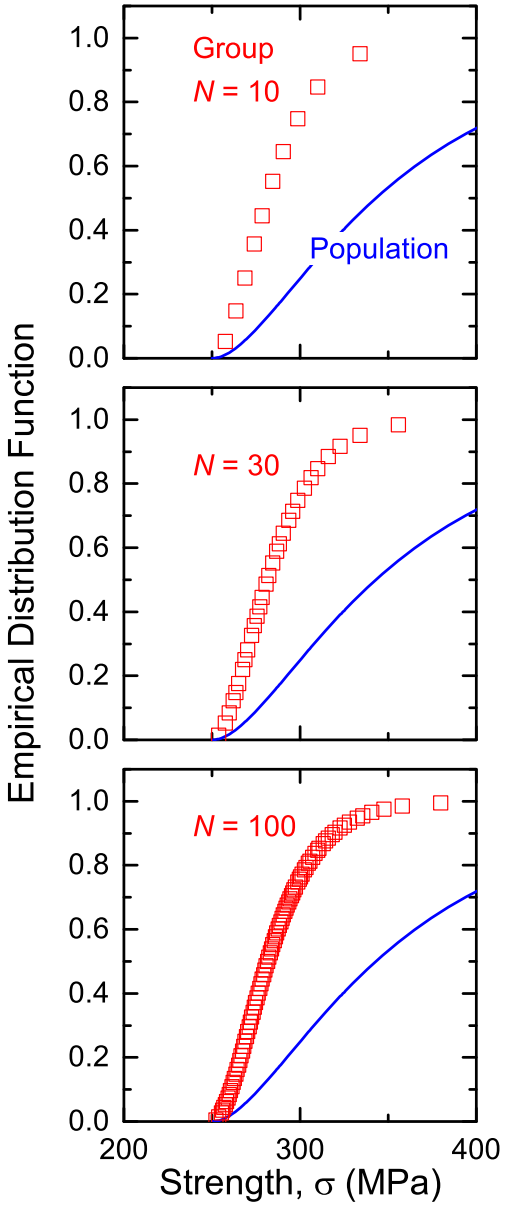

Fig. 5 Plot of the strength empirical distribution function for groups of components of fixed volume ($k = 5$) but various numbers of components within the group, N. The cdf of the population is shown as the lines ($k = 1$, $N >> 1$, Fig. 4). At small group numbers (small N), the group strength empirical distribution function is significantly truncated at large strengths away from the population cdf but the threshold remains well defined

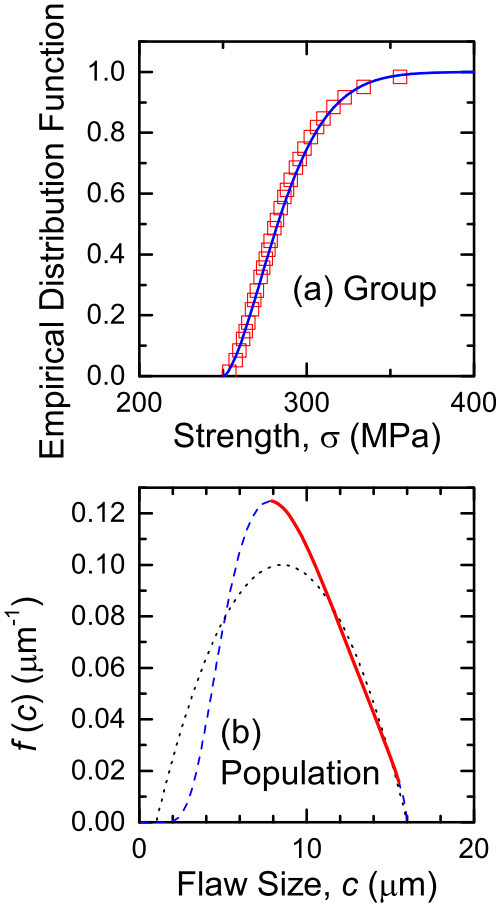

Fig. 6 **(a)** Plot of the strength empirical distribution function for a group of $N = 30$ components drawn from the quadratic flaw-size population (symbols, $k = 5$, Fig. 5(b)) and a fit of the Weibull distribution function $F_{\text{group}}(\sigma)$ (line, equation (13)). **(b)** Plot of the flaw-size pdf $f(c)$ inferred from the Weibull $F_{\text{group}}(\sigma)$ fit, dashed line, equation (17); the bold solid line shows the domain of flaw sizes conjugate to the domain of observed strengths. The underlying quadratic population is shown as the dotted line, equation (1), Fig. 2(a). Only at large flaw sizes is there agreement

"group" in equation (13) indicates that this is a group-specific function (the related "V" is not used as V is usually not known). m is a group-specific exponent and σ_{th} and σ_θ are group-specific strength parameters; the exponent and strength parameters are obtained by fitting to $P_i(\sigma_i)$ for a group of components. An example is shown in Fig. 6(a), in which equation (13) was visually fit to the $k = 5$, $N = 30$ group from the simple quadratic example, constrained only by the known $\sigma_{\text{th}} = 250$ MPa, resulting in $m = 1.60$ and $\sigma_\theta = 41.0$ MPa (the "characteristic strength" is $\sigma_{\text{th}} + \sigma_\theta = 291.0$ MPa).

Explicit quantitative determination of the underlying flaw population from a Weibull cdf fit begins with recognizing that the Weibull ccdf complementary to the above cdf is, similar to equation (12),

$$\overline{F}_{\text{group}} = 1 - F_{\text{group}}(\sigma) = \exp\left[-\left(\frac{\sigma - \sigma_{th}}{\sigma_\theta}\right)^m\right]$$

By implication, the ccdf for the population is of the same form (equation (10)),

$$\overline{F}(\sigma) = \exp\left[-\left(\frac{\sigma - \sigma_{\text{th}}}{\sigma_0}\right)^m\right] \tag{14}$$

where m, σ_{th} and σ_0 are parameters describing the element population over the region $\sigma \geq \sigma_{\text{th}}$. (The simple form of this equation enables inhomogeneous loading to be easily studied—see Appendix) The scaling parameter for the population, σ_0, is related to the scaling parameter of the group, σ_θ, by the component volume

$$(\sigma_\theta)^m = (\sigma_0)^m/k, \tag{15}$$

and this relationship can be used to scale the Weibull distribution between groups of different volume components. The group cdf above is often written in terms of population distribution and component volume terms rather than a mix of population and group terms,

$$F_{\text{group}}(\sigma) = 1-\exp\left[-k\left(\frac{\sigma-\sigma_{\text{th}}}{\sigma_0}\right)^m\right]$$

Note that it is not dimensionally correct to replace k by V, although this is common (as it makes it clear that strengths should decrease as component size increases, but conflates the Weibull distribution with the unrelated independent element assumption and requires σ_0 to have dimensions other than stress). Use of the known $k = 5$ gives $\sigma_0 = 112$ MPa here, equation (15).

The well-known population strength pdf conjugate to the above population cdf [5], using equations (8) and (14), is

$$f(\sigma) = \frac{m}{\sigma_0}\left(\frac{\sigma-\sigma_{\text{th}}}{\sigma_0}\right)^{m-1}\exp\left[-k\left(\frac{\sigma-\sigma_{\text{th}}}{\sigma_0}\right)^m\right]$$

This is known as the Rosin-Rammler distribution [44], when used to describe particle or fragment size. The inverse relationship between strength and flaw size substituted into the ccdf relation gives the Weibull-idealized form for the flaw population cdf

$$F(c) = \begin{cases} \exp\left[-\left(\dfrac{c^{-1/2}-c_{\max}^{-1/2}}{c_0^{-1/2}}\right)^m\right], & 0\le c\le c_{\max} \\ 1, & c > c_{\max} \end{cases}. \tag{16}$$

Thus, the Weibull-idealized population flaw size pdf is

$$f(c) = \begin{cases} \exp\left[-\left(\dfrac{c^{-1/2}-c_{\max}^{-1/2}}{c_0^{-1/2}}\right)^m\right]\left(\dfrac{c^{-1/2}-c_{\max}^{-1/2}}{c_0^{-1/2}}\right)^{m-1}\dfrac{m(c/c_0)^{-3/2}}{2c_0}, & 0\le c\le c_{\max} \\ 0, & c > c_{\max} \end{cases} \tag{17}$$

shown as the dashed line in Fig. 6(b) (using $B = 1.0$ MPa m$^{1/2}$, $c_0 = 79.7$ μm and $c_{\max}$ is unaltered). The idealized flaw-size pdf has a bounded region of support, unlike the Weibull strength pdf. The experimental flaw-size pdf is bounded by the measured strengths and is shown in Fig. 6(b) as the solid line. For reference, the underlying quadratic flaw-size pdf, equation (1), Fig. 2(a), is reproduced as the dotted line.

A Weibull distribution fit to a group of component strengths, Fig. 6(a), gives rise to an inferred population of flaw sizes that agrees with the known population at large flaw sizes, but which disagrees at small flaws, Fig. 6(b). The disagreement in this case is a consequence of a lack of constraint on the Weibull fit at large strengths due to the contracting and truncating effects discussed above. The contraction and truncation effects are also evident in the domain of flaw sizes over which the deconvoluted population pdf is supported by the strength observations: in this case it was about half the known domain, at large flaw sizes. To obtain a reliable estimate of the small-flaw end of the flaw pdf, Weibull or otherwise, a very large group of components, many more than commonly used or used here, is required (assuming small k).

At a fundamental level, however, the required form of the pdf, equation (17), for the population of flaws generated by a manufacturing process and ultimately responsible for a Weibull distribution of component strengths is not intuitive: it is not a power law [10, 22, 35, 40] or an exponential, or a power law-exponential product [12–14]. That is, it seems unlikely that any model of any manufacturing process would give rise to a population of flaws given by equation (17). It seems unlikely then, that the Weibull-form cdf for a group of strengths has any fundamental basis in a pdf for a population of flaws generated by a manufacturing process. An important exception to this statement is that a threshold in the strength cdf is clearly associated with a maximum in the flaw pdf.

Example: Experimental Applications

The analysis above provides the connection between a material flaw population and a component strength distribution. Insight was provided by considering mathematically simple flaw population and component strength expressions that described simple forms, parabolic and sigmoidal, respectively. In cases in which the forms are not simple, perhaps requiring complicated mathematical expressions, or representing experimental data, the connections between flaw population and strength distribution must be made numerically (e.g., [12]). Three example applications of the above framework to experimental data are provided here, using numerical analysis following the analytical example of Fig. 6 and gradually increasing in complexity. The first example considers two micro-scale components of Si MEMS test structures characterized by unimodal flaw populations. This is the simplest example, illustrating state-of-the-art data with large N and changes in f. The second example considers another set of Si MEMS structures characterized by a known bimodal flaw population with moderately large N. The third example considers SiNWs that have undergone various oxidation steps leading to changes in both f and k, and tested with small N. In these examples, analysis proceeds in the reverse direction by beginning with the experimental strength distributions of groups of components and inferring the underlying flaw populations for comparison with independent observations. Each example took minutes to analyze using commercial software on a desktop computer.

Si MEMS Structures: Unimodal Flaws

The application of the reverse analysis procedure is part of a conventional manufacturing process and enables "what is" questions to be answered. The question here: "What is the flaw population corresponding to a measured strength distribution?" The measured strength distributions taken here result from tensile tests on Si components formed by typical dry-etch MEMS manufacturing processes and featured in a recent review of MEMS strengths [8]; details are given elsewhere [5, 6]. Briefly, the first group of components were $N=$ 1008 polycrystalline Si bars about 2.0 μm × 2.25 μm in cross section and 20 μm long. The second group of components were $N=209$ single-crystal Si bars about 25 μm × 8 μm in cross section and 250 μm long.

Figures 7(a) and 7(b) show the empirical distribution functions $P_i(\sigma_i)$ of the component strengths. Symbols represent individual measurements. The solid lines represent best-fit Weibull distributions [5, 6], equation (13), to the groups, limited to the empirical regions of support, about 2.0 GPa to 3.2 GPa and 1.4 GPa to 3.2 GPa, respectively. The fits are good, representing smoothed sigmoidal forms of the strength data, although there are some deviations in places. The conjugate domains for the empirical flaw-sizes were about 60 nm to 160 nm and 270 nm, respectively, using $B=0.75$ MPa $m^{1/2}$ [8] in equation (4). $f(c)$ variations for the populations of flaws, using $k=3$, are shown in Figs. 7(c) and 7(d): symbols represent individual determinations at the flaw-size indicated; the solid lines represent the determinations from the (smoothed) Weibull fits to the strength data limited to the empirical domains of flaw sizes. (The exact value of k is unknown and hence $k=3$ was used here for ease of comparison between groups and with the analytical work above. Experiments on identically-processed but different size components are required to estimate k. The value chosen does not influence the findings.)

The first point to note in Figs. 7(c) and 7(d) is that the scatter in the individual data about the smoothed fit is considerable; a consequence of taking derivatives over expanded domains ($c \sim \sigma^{-2}$), even of data with only small deviations from smoothness, Figs. 7(a) and 7(b). The smoothed trends indicate asymmetric material flaw population pdfs consisting of single "wings" with modes at approximately the minimum values and extending by about a factor of five to the maximum values, similar to Fig. 6. The uncertainties in the peaks of the *smoothed* distributions are approximately the widths of the smoothed lines, consistent with the fits to the raw strength data, Figs. 7(a) and (b). The second point is that the flaw distribution in Fig. 7(d) is broader than that in Fig. 7(c), reflecting different processing procedures. These behaviors are less discernible from the individual data and hence a great benefit of the smooth Weibull fits is to display underlying trends (other smoothing schemes, e.g., normal distribution, [45, 46] would provide the same benefit). Both the raw and smoothed flaw-size data much better estimate the large-flaw pdf than the small-flaw pdf, for which there is no information for flaws smaller than about 50 nm. Using the experimental data in Fig. 7 highlights that the relationship between a material flaw population (in this case, inferred to be asymmetric within scatter) and the resulting strength distribution of a group of components (here, symmetric and relatively smooth) is not intuitively obvious.

A third, important, point is that the sizes of the strength-controlling flaws in Fig. 7 are much larger than the surface features identified in independent atomic force microscopy (AFM)-based topography measurements on these materials [6, 47]. Grain-boundary grooves about 1 μm apart with depths >15 nm were observed on the surface of the polycrystalline material from the first group [47]. Surface roughness with about 40 nm peak-to-valley amplitude was observed on the surface of the single-crystal material from the second group [6]. No features were observed in the flaw size ranges of Fig. 7. The implication is that the strength controlling flaws were present but not observed in these measurements, most likely because of the limited AFM scan areas. Hence, the manufacturing parameter λ, the density of *strength-controlling* flaws, is small and not well represented by topographic observations and, conversely, ΔV is large. The difference between small- and large-scale topographic features was noted in a roughness study of MEMS surfaces [48], as was the lack of correlation of strengths with small-scale features, as noted here. The test component parameter k is also small, consistent with values used above, and small λ and k are consistent with the independent element assumption [36–39] and the *lack* of step-functions in $F_V(\sigma)$, appearing in Fig. 4 for large k.

Si MEMS Structures: Bimodal Flaws

The second set of measured strengths also resulted from tensile tests on Si components formed by dry-etch MEMS manufacturing processes [8, 49]. The set consisted of $N=$ 105 single-crystal Si bars about 25 μm × 8 μm in cross section and 250 μm long. The set included bars with regular, small, surface scallops formed by the intentional etching process and bars with irregular, larger, surface pitting formed by an unintentional etching process. The bars were formed in the same manufacturing cycle and separated into the scallops and pitting sub-populations by independent dimensional measurements; details are given elsewhere [49].

Figure 8(a) shows the empirical distribution function $P_i(\sigma_i)$ of the component strengths. Symbols represent individual measurements; the scallops (mostly large strengths) and pitting (mostly small strengths) are indicated by different symbols. The strength overlap region is indicated by a

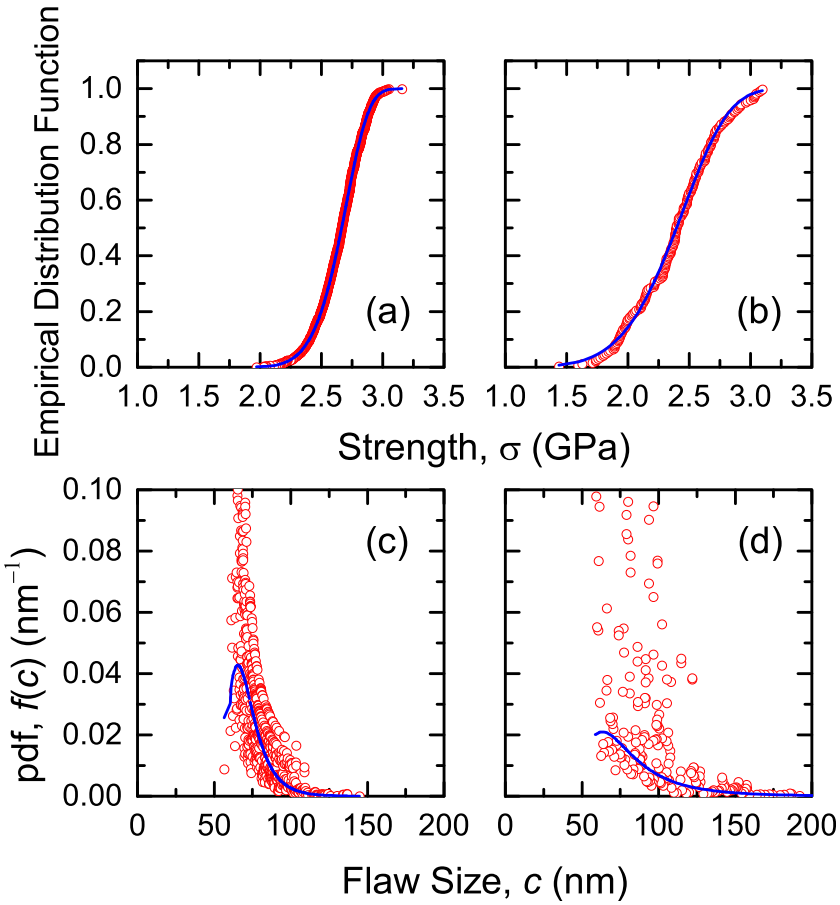

Fig. 7 **(a)** Plot of the strength empirical distribution function for a group of polycrystalline Si MEMS components. Symbols are individual strength measurements, line is best-fit Weibull smoothing function. **(b)** Plot of the strength empirical distribution function for a group of single-crystal Si MEMS components. Notation as in **(a)**. **(c)** Plot of the population flaw-size pdf inferred from **(a)**. Symbols and line as in **(a)**. **(d)** Plot of the population flaw-size pdf inferred from **(b)**. Symbols and line as in **(b)**

shaded band. The bimodal nature of the distribution is indicated by the inflection within the overlap region separating two sigmoids. The complete bimodal region of support was about 1.0 GPa to 2.5 GPa and the conjugate domain for the flaw-sizes was about 70 nm to 1000 nm using $B =$ 0.75 MPa $m^{1/2}$ [8] in equation (4). $f(c)$ variations for the population of flaws, using $k = 3$, are shown in Fig. 8(b): different symbols represent the different surface finishes with scallops mostly small flaws and pitting mostly large flaws. The shaded band once again indicates the overlap region. Although there is considerable scatter as in Fig. 7, it seems clear that there are two flaw populations: one sub-population of large pitting flaws peaked to the right of the overlap band and another sub-population of small scallop flaws peaked to the left of the overlap band. This explicit calculation of bimodal flaw sizes greatly extends the earlier speculation based on the strength measurements. As above, the size of the strength-controlling flaws in Fig. 8 is much larger than the sizes of the observed topographic features, in this case about 35 nm to 200 nm. The implication is the same as above, the strength-controlling features were not observed due to AFM scan limitations and that λ and k are small. An extreme example of widely-separated flaw sub-populations is shown in experiments on paper strips [42].

SiNWs

The final sets of strength distributions considered here result from bending tests on SiNWs formed by vapor-liquid-solid growth. Mean strengths—approaching the theoretical values—and structures as a function of oxidation time were considered elsewhere [50]. Briefly, the SiNWs were about 25 μm long × 70 nm in diameter, consisting of cylindrical Si cores and annular section SiO_2 shells, in groups of $N = 10$ to 11 wires of different oxidation time and shell thickness; the overall SiNW radius increased with oxidation time. The strengths were determined from a non-linear analysis of the bending curvature at failure.

Figure 9(a) shows the empirical distributions of the groups of SiNW strengths. The distributions are all steep, barely sigmoidal, and the native SiNWs are twice as strong (about 20 GPa) as the oxidized wires (about 10 GPa), which exhibit a non-monotonic trend in strength with oxidation time (rapid decrease followed by gradual increase); the legend in Fig. 9(b) is common to both plots. The conjugate domains for the empirical flaw sizes were about 1 nm to 10 nm, using $B =$ 0.75 MPa $m^{1/2}$ for the native wires and 0.5 MPa $m^{1/2}$ for the oxidized wires [8, 50]. The $f(c)$ variations were calculated by assuming surface flaws and scaling k with wire diameter,

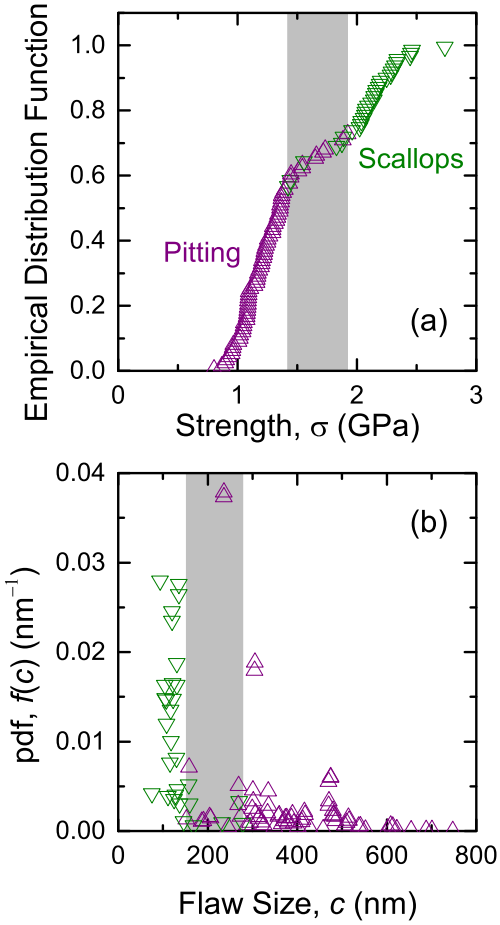

Fig. 8 **(a)** Plot of the strength empirical distribution function for a group of single-crystal Si MEMS components consisting of a bimodal population of flaws: an uncontrolled pitting etch and and a controlled scallop etch. Different symbols indicate the different etch populations and the shaded band indicates the region of strength overlap. **(b)** Plot of the population flaw-size pdf inferred from **(a)**. Symbols as in **(a)**. The shaded band indicates the region of flaw-size overlap

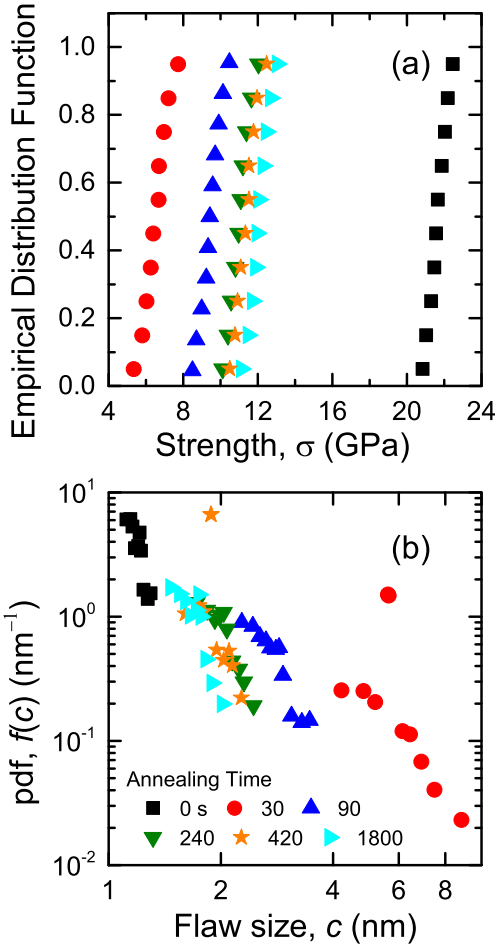

Fig. 9 **(a)** Plot of the strength empirical distribution functions for groups of native and oxidized SiNWs. Symbols are individual strength measurements. **(b)** Plot of the population flaw-size pdfs inferred from **(a)**. Legend in **(b)** indicates annealing (oxidation) times

increasing from $k = 3$ for the native wires to $k = 4.5$ for the maximally-oxidized wires [50]. The $f(c)$ variations are shown in Fig. 9(b) (using a logarithmic scale for ease of display). The small N effects severely limit the information that can be obtained about the flaw populations: In each case, the inferred flaw population consists of a single wing truncated at the peak, although it is clear that the unoxidized wires have very small flaws, that initial oxidation greatly increases the flaw size, and that further oxidation gradually decreases the flaw size.

A likely scenario is that the strengths of the native wires are controlled by near-atomic scale flaws in the Si. On initial oxidation, inhomogeneous patches of oxide form on the surface of the wires and strengths are controlled by large flaws at the Si-oxide patch edges and corners. On further oxidation, the oxide coating becomes continuous and the strengths are controlled by smaller flaws on the oxide surface. In this case, the size of the strength-controlling flaws is comparable to the observed topographic features arising from the growth and oxidation processes. Fig. 10 shows AFM surface height traces along the lengths of the SiNWs: For both the strongest (native) and weakest (initial oxidation) SiNWs the correlation between the peak-to-valley variation in the surface topography and the strength-controlling flaw size is clear, about 1.2 nm for the native SiNWs and about 6 nm for the initially oxidized SiNWs. The implication here is that the observed topography *is* representative of the strength-controlling flaws because the AFM scans are comparable to the stressed areas. Noting that the extremes of topography vary over about 100 nm in Fig. 10 and that the extremes of the tensile stresses generated in the bent wires extended over 5 to 10 SiNW diameters [50], about 350 nm to 700 nm, the estimate of the effective sample size of $k = 3$ to 4.5 is appropriate.

Discussion

The above analysis provides a clear and unambiguous path from the fundamental flaw-size population pdf, $f(c)$,

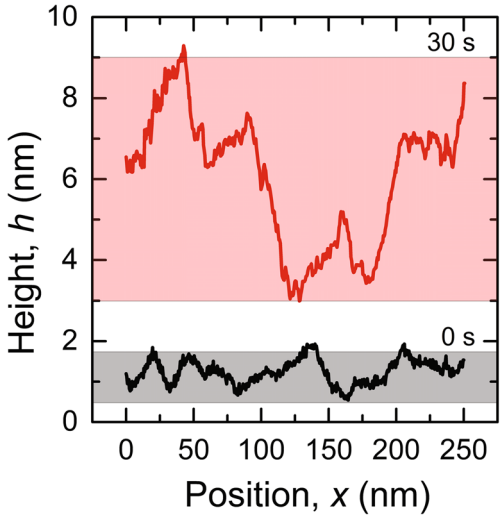

Fig. 10 AFM topographic data taken along the length of SiNWs (lines) and average flaw sizes taken from Fig. 9 (shaded bands)

characterizing a manufactured material, to an empirical distribution function, $P_i(\sigma_i)$, describing the strengths of a selected group of components. In following this forward analysis path, $f(c) \rightarrow F(c) \rightarrow \overline{F}(\sigma) \rightarrow F_V(\sigma) \rightarrow P_i(\sigma_i)$, the assumptions and effects regarding the strength-flaw-size relationship, the volume of the components, and the number in the group, were all made clear. In particular, the contracting effects of component volume in the $\overline{F}(\sigma) \rightarrow F_V(\sigma)$ step and the truncating effects of group number in the $F_V(\sigma) \rightarrow P_i(\sigma_i)$ step were noted. Many of the ideas and assumptions in the analysis have been included in the extensive previous works on this subject: the probabilistic independence of elements assumption (the weakest link hypothesis) [36–39]; the identification of the population flaw size cdf with the population strength ccdf ($F(c) \rightarrow \overline{F}(\sigma)$, and vice versa) [12, 13, 15, 22, 32–35]; the recognition that the empirical distribution function is a statistical estimator of the underlying group cdf ($P_i(\sigma_i) \rightarrow F_V(\sigma)$, see below); that specialized MEMS test structures are required to provide such estimation [2–7]; and, that reverse or inverse analysis is possible [16]. The analysis here clearly separates these ideas with a minimum of notation within the well-established concepts of probability [26] and allows for new experimental interpretation.

The reverse analysis path, leading from an experimental measurement of a group of strengths to the underlying population of flaws, $f(c) \leftarrow P_i(\sigma_i)$, was also clear and unambiguous and subject to the same assumptions and effects. This might be the most important part of the analysis and answers the original question. In general, truncation and contraction effects lead to an incomplete specification of $f(c)$ from $P_i(\sigma_i)$ and in particular the small flaw region of the flaw population is not specified. However, truncation effects do not affect the large flaw region at all and contraction effects enhance the ability to specify the large flaw region. The threshold strength is very well estimated by component strength measurements and as a consequence the maximum flaw in the manufactured population is also well estimated, Figs. (4, 5, 6, 7, 8 and 9). Both of these parameters are of direct use to designers and manufacturers. Using a margin of safety, a designer can use the threshold strength and its uncertainty directly in design calculations for components manufactured with the same process as the test components. Manufacturers can use the maximum flaw size to identify mechanisms leading to the largest flaws and alter processing parameters accordingly. The importance of the threshold, beyond its use as a descriptive fitting parameter [5, 36], in characterizing processing effects [7] and in design [5, 8], has been so far little noted.

With the exception of the threshold, it is difficult to see how strength measurements of components can provide a good estimate of the flaw population of manufactured materials. Deconvolution of $P_i(\sigma_i)$ from measurements on a sampled group of components to obtain quantities characterizing the underlying population is hampered by several factors: First, $k > 1$ contracts the domain over which strengths are observed to vary significantly and hence limits the ability to fit experimental data to an analytical form. The domain is bounded at small strengths, however, by the threshold. Second, finite N truncates the domain by eliminating large strengths, again limiting fitting ability. Third, unknown k precludes exact connection between the group ccdf and the population ccdf. The first and second of these largely affect deconvolution precision and the third largely affects accuracy: see Fig. 6. Precision is further degraded by the derivative nature of the reverse transformation $f(c) \leftarrow F(c)$: see Fig. 7. An even further effect, on accuracy, is that, even if the population strength cdf is well estimated, knowledge of the strength-flaw size relationship $F(c) \leftarrow \overline{F}(\sigma)$ is required to specify the population flaw-size pdf and thence infer manufacturing and design choices (e.g., notches [51] rather than cracks would result in a different $\sigma(c)$ dependence). Overcoming the contraction and truncation issues would seem to favor MEMS-based samples by using small test components (small k) tested in large numbers (large N) [e.g., 5,7] and this is the focus of current research. In prior published experiments, [7] implicit determination of $f(c)$ was used in predicting strength distributions of MEMS samples adjusting for threshold variations and using a range of k values (enhanced by the use of stress concentrating notches). In particular, these experiments showed that larger component size range will improve parameter estimation by enabling a wider strength range. Another suggestion is that small-enough k could reduce N to manageable values to obtain the required uncertainty in explicit determination of $f(c)$ [40, 46].

Unsurprisingly, given the above points, the Weibull distribution function has played little role in the above analysis. In Fig. 6, the Weibull function has been used as a convenient demonstration of the effects of extrapolation and in Fig. 7 it has been used as a convenient smoothing function. In both cases, as all unimodal pdfs produce sigmoidal cdfs, any

sigmoid would have fulfilled the requirements. Conversely, the flexibility in the sigmoidal shape of a Weibull cdf can be used to describe the strength distribution of many (non-Weibull) unimodal flaw pdfs [e.g., 12,13]. The analysis above thus affirms many of the points of Todinov [42, 52] and Zok [53]: Strength (or electrical breakdown [41]) distributions need not be Weibull-like; the Weibull function(s) have nothing to do with weakest link or independence of element ideas, equation (10); the Weibull functions are not fundamental in the sense of derivability, equation (17); and, the flexibility in the Weibull sigmoid cdf leads to apparently good fits for small data sets far from the upper bound of a group, equation (13), leading to the idea that there is some underlying physical significance. With regard to this last point, the empirical choices of m and σ_θ enable equation (13) to fit the data from many groups of components (not only strengths). The application often involves linearization of equation (13) into the form $y = ax + b$ by setting $\sigma_{\text{th}} = 0$, $y = \ln[\ln(1/(1 - F))]$, and $x = \ln\sigma$, and similar transformation of the $P_i(\sigma_i)$ parameters by $\ln[\ln(1/(1 - P_i))]$, and $x = \ln\sigma_i$; fitting a straight line then gives $m = a$ and $\ln\sigma_\theta = b/a$. The contracting double-logarithmic transformation causes nearly all data sets to approximate a straight line; the straightening effect is exacerbated in this case by k and N effects leading to data contraction and truncation as described above. Data are often plotted in transformed coordinates and straight-line behavior in such plots presented in support of the two-parameter (threshold-less) equation (13). If the data do not form a straight line, the formulation is often enforced on limited domains, requiring $m = m(\sigma)$ [20]. (Weibull allowed for non-zero σ_{th} [36, 37], but the historical apparent simplicity and applicability of the two-parameter linearization have largely led to zero threshold analyses.) Empirically, large values of σ_θ are associated with large strengths and large values of m are associated with small strength variability. The extrapolation from strength tests on a group of components to estimation of the population of manufactured flaws is usually implicit and qualitative; large σ_θ and m are "good" as they represent small flaws and little flaw variability.

Conclusions

The analytical connection between a manufactured flaw population and a sampled component strength distribution is clear and simple: forward analysis permits strength distributions to be predicted theoretically and reverse analysis permits flaw populations to be estimated experimentally. Analysis suggests strength-controlling flaw densities are small and that strength-controlling flaws are larger than most topographic observations would suggest. The analysis strongly supports the weakest link hypothesis but shows that the Weibull function is not related to this hypothesis and is not necessary for strength analysis. Some open questions fall into the two categories of forward and reverse analysis: First, the application of the forward analysis procedure in the manufacturing process enables "what if" questions to be answered. The questions here are "What do strength distributions look like if flaw populations are asymmetric? bimodal? multimodal? [42, 53] and what if the component were a different size [40]?" For example, the bimodal flaw population could represent a process that results in a majority population of typical manufacturing flaws and a minority population of large flaws ("outliers") and extrapolation from test size to component size will always be required. Second, and more important, a variety of statistical techniques enable strength thresholds to be better estimated using analyses of strength distributions. For example, confidence intervals for threshold strengths and the conjugate maximum flaw sizes could be estimated assuming a range of assumed distributions, providing more confidence to manufacturers of nano- and micro-scale components about the outcomes of limited strength tests.

Acknowledgements The authors appreciate helpful discussions with Brad L. Boyce of Sandia National Laboratories on this topic and his provision of the raw data for Fig. 7(a); support for BLB was provided by the Center for Integrated Nanotechnologies. The authors also appreciate helpful discussions with Lawrence H. Friedman and Antonio M. Possolo, both of NIST.

Appendix: Inhomogeneous Loading

For a component composed of M discreet sub-volumes V_i, such that $\sum_i^M V_i = V$ where i is a sub-volume index, and each sub-volume consists of k_i elemental volumes such that $V_i = k_i \Delta V$ and thus $\sum_i k_i = k$, the independent probability assumption gives the component ccdf as

$$\overline{F}_V(\sigma) = \overline{F}(\sigma)^{k_1}\overline{F}(\sigma)^{k_2}\ldots\overline{F}(\sigma)^{k_M}$$

If each sub-volume is held to a separate strength exceedance, σ_i, the overall component exceedance is

$$\overline{F}_V(\sigma_i, k_i) = \overline{F}(\sigma_1)^{k_1}\overline{F}(\sigma_2)^{k_2}\ldots\overline{F}(\sigma_M)^{k_M}$$

for the specified configuration. The exceedance can thus be written as a logarithmic sum

$$\begin{aligned}\ln\left[\overline{F}_V(\sigma_i, k_i)\right] &= \sum_i^M \ln\left[\overline{F}(\sigma_i)\right]k_i \\ &= \lambda\sum_i^M \ln\left[\overline{F}(\sigma_i)\right]V_i\end{aligned}$$

where the second line makes clear that the sum is over the volume of the component and $\lambda = 1/\Delta V$ is the number density of elements (and thus flaws) per volume.

If V_i and thus ΔV are reduced in size to the infinitesimal limit (and λ is still defined) such that the component can be regarded as a continuum, each *point* can be held to separate strength exceedance, $\sigma(x, y, z)$, where (x, y, z) is a point coordinate in the component. The sum above thus becomes an integral

$$\ln\left(\overline{F}_V\right) = \lambda \int_V \ln\left[\overline{F}(\sigma; x, y, z)\right] \mathrm{d}V$$

where $\overline{F}_V$ is understood to be configuration dependent. If the exceedance is constant, the integral collapses to a product and gives the oft-cited result $F_V = 1 - \exp[\lambda V \ln(1 - F)]$, [42, 52, 54] recognizing that $F = 1 - \overline{F}$. The full equation can be reduced in complexity considerably: (1) If a plane (say, *x*-*y*) of fixed area is held to a separate exceedance such that $\sigma = \sigma(z)$ only and $\mathrm{d}V = \mathrm{d}x\mathrm{d}y\mathrm{d}z = A_{xy}\mathrm{d}z$, where A_{xy} is the area of the plane. Thus

$$\overline{F}_V = \exp\left[\mu \int_Z \ln\left[\overline{F}(\sigma; z)\right] \mathrm{d}z\right],$$

where $\mu = \lambda A_{xy}$ is the number density of flaws/length along z in the plane; (2) If a simple form is selected for $\ln\left(\overline{F}\right)$, say the Weibull distribution with $\sigma_{\mathrm{th}} = 0$ such that $\ln\left(\overline{F}\right) = -(\sigma/\sigma_0)^m$. Thus

$$\overline{F}_V = \exp\left[-\frac{\mu}{\sigma_0^m} \int_Z (\sigma; z)^m \mathrm{d}z\right]$$

and, (3) If a simple form is selected for σ, say the outer-fiber tensile stress in a built-in cantilever beam of length L, supporting a weight w at the free end, such that $\sigma = wz/Z$, where Z is the section modulus of the beam perpendicular to z. Thus

$$\begin{aligned} F_L(w) &= 1 - \exp\left[-\mu\left(\frac{w}{Z\sigma_0}\right)^m \int_0^L z^m \mathrm{d}z\right] \\ &= 1 - \exp\left[-\frac{\mu L}{(m+1)}\left(\frac{wL}{Z\sigma_0}\right)^m\right] \end{aligned}$$

similar to an earlier derivation [55]. The analogous expression for a homogeneous rod of cross section A, uniformly loaded in tension by weight w, is

$$F_L(w) = 1 - \exp\left[-\mu L A\left(\frac{w}{A\sigma_0}\right)^m\right]$$

The group cdf $F_L(w)$ gives the proportion of beams or rods of length L that fail under weight w; the probability of failure is now expressed in terms of the extensive variables of failure weight and component size, rather than the intensive variable of strength σ.

In both inhomogeneous and homogeneous configurations, the variation of the cdf with the failure variable w is identical. The form of the distribution is unaffected by the mode of loading. However, in the case of inhomogeneous loading, (unsurprisingly) there is a much greater dependence on the geometry of the component: In the case of the beam in bending, an additional dependence on beam length and details of the shape of the cross-section appear in the cdf, whereas for the tensile rod, only the area of the cross section appears. Note also that the flaw-population exponent appears twice in the inhomogeneous cdf. The magnitude of the distribution is thus strongly affected by the geometry of the component in inhomogeneous loading. The extreme opposite to the simple case considered above is a stochastic distribution of stress superposed on the stochastic distribution of strengths [51].

References

1. Ashby MF (1999) Materials selection in mechanical design. Butterworth-Heinemann, Oxford, UK. https://doi.org/10.3758/BF03210826
2. Namazu T, Isono Y, Tanaka T (2000) Evaluation of size effect on mechanical properties of single crystal silicon by nanoscale bending test using AFM. J Microelectromech Syst 9:450–459. https://doi.org/10.1109/84.896765
3. Fitzgerald AM, Pierce DM, Huigens BM, White CD (2009) A general methodology to predict the reliability of single-crystal silicon MEMS devices. J Microelectromech Syst 18:962–970. https://doi.org/10.1109/JMEMS.2009.2020467
4. Naraghi M, Ozkan T, Chasiotis I, Hazra SS, de Boer MP (2010) MEMS platform for on-chip nanomechanical experiments with strong and highly ductile fibers. J Micromech Microeng 20: 125022-1–125022-9
5. Boyce BL (2010) A sequential tensile method for rapid characterization of extreme-value behavior in microfabricated materials. Exp Mech 50:993–997. https://doi.org/10.1007/s11340-009-9286-x
6. Gaither MS, Gates RS, Kirkpatrick R, Cook RF, DelRio FW (2013) Etching process effects on surface structure, fracture strength, and reliability of single-crystal silicon theta-like specimens. J Microelectromech Syst 22:589–602. https://doi.org/10.1109/JMEMS.2012.2234724
7. Saleh ME, Beuth JL, DeBoer MP (2014) Validated prediction of the strength size effect in polycrystalline silicon using the three-parameter Weibull function. J Am Ceram Soc 97:3982–3990. https://doi.org/10.1111/jace.13226
8. DelRio FW, Cook RF, Boyce BL (2015) Fracture strength of micro- and nano-scale silicon components. Appl Phys Rev 2:021303–1–021303–51
9. Yole Développment (2017) Overview of the MEMS and sensor market for automotive. http://www.yole.fr/iso_album/illus_mems_sensors_for_automotive_marketoverview_yole_aug2017.jpg Accessed 12/12/2017
10. Hild F, Marquis D (1992) A statistical approach to the rupture of brittle materials. Eur J Mech A/Solids 11:753–765
11. Danzer R, Lube T, Supancic P (2001) Monte Carlo simulations of strength distributions of brittle materials – type of distribution, specimen and sample size. Z Metallkd 92:773–783
12. Jayatilaka Ade S, Trustrum K (1977a) Statistical approach to brittle fracture. J Mater Sci 12:1426–1430

13. Jayatilaka Ade S, Trustrum K (1977b) Application of a statistical method to brittle fracture in biaxial loading systems. J Mater Sci 12: 2043–2048
14. Sigl LS (1992) Effects of the flaw distribution function on the failure probability of brittle materials. Z Metallkd 83:518–523
15. Danzer R (1992) A general strength distribution function for brittle materials. J Eur Ceram Soc 10:461–472
16. Ahn Y, Nicholson DW, Wang MC, Ni P (2000) Inverse method for identifying the underlying crack distribution in plates with random strengths. Acta Mech 144:137–154. https://doi.org/10.1007/BF01170171
17. Poloniecki JD, Wilshaw TR (1971) Determination of surface crack size densities in glass. Nature Phys Sci 229:226–227. https://doi.org/10.1038/physci229226a0
18. Wilshaw TR (1971) The Hertzian fracture test. J Phys D Appl Phys 4:1567–1581. https://doi.org/10.1088/0022-3727/4/10/316
19. Warren PD (1995) Statistical determination of surface flaw distribution in brittle materials. J Eur Ceram Soc 15:385–394
20. Warren PD (2001) Fracture of brittle materials: effects of test method and threshold stress on the Weibull modulus. J Eur Ceram Soc 21:335–342
21. Tandon R, Paliwal B, Gibson C (2013) Practical aspects of using Hertzian ring crack initiation to measure surface flaw densities in glasses: influence of humidity, friction and searched areas. Phil Mag 93:2847–2863. https://doi.org/10.1080/14786435.2013.790567
22. Hunt RA, McCartney LN (1979) A new approach to Weibull's statistical theory of brittle fracture. Int J Fracture 15:365–375
23. Graham-Brady L (2010) Statistical characterization of meso-scale uniaxial compressive strength in brittle materials with randomly occurring flaws. Int J Solids Struct 47:2398–2413. https://doi.org/10.1016/j.ijsolstr.2010.04.034
24. Kinsella DT, Persson K (2018) A numerical method for analysis of fracture statistics of glass and simulations of double ring bending test. Glass Struct Eng 3:139–152. https://doi.org/10.1007/s40940-018-0063-z
25. Chao L-Y, Shetty DK (1992) Extreme-value statistics analysis of fracture strengths of a sintered silicon nitride failing from pores. J Am Ceram Soc 75:2116–2124. https://doi.org/10.1111/j.1151-2916.1992.tb04473.x
26. Walpole RE, Myers RH (1972) Probability and statistics for engineers and scientists. Macmillan Publishing Co., Inc., New York
27. Lawn BR (1993) Fracture of brittle solids, 2nd edn. Cambridge University Press, Cambridge
28. Hartzell AL, da Silva MG, Shea HR (2011) MEMS Reliability. Springer, New York
29. Wikipedia, Cumulative distribution function. https://en.wikipedia.org/wiki/Cumulative_distribution_function Accessed 12/12/2017
30. Bertrand PT, Laurich-McIntyre SE, Bradt RC (1988) Strengths of fused and tabular alumina refractory grains. Am Ceram Soc Bull 67:1217–1222
31. Brzesowsky RH, Spiers CJ, Peach CJ, Hangx SJT (2011) Failure behavior of single sand grains: theory versus experiment. J Geophys Res 116:B06205–1–B0620513
32. Hunt RA (1978) A theory of the statistical linking of microcracks consistent with classical reliability theory. Acta Metall 26:1443–1452. https://doi.org/10.1016/0001-6160(78)90159-1
33. McCartney LN (1979) Extensions of a statistical approach to fracture. Int J Fracture 15:477–487. https://doi.org/10.1007/BF00023333
34. Trustrum K, Jayatilaka Ade S (1983) Applicability of Weibull analysis for brittle materials. J Mater Sci 18:2765–2770. https://doi.org/10.1007/BF00547593
35. Hild F, Marquis D (1990) Correlation between defect distribution and failure stress for brittle materials. C R Acad Sci Paris 311:573–578 (in French)
36. Weibull W (1939) A statistical theory of the strength of materials. Ingeneiördsvetenskapsakademiens 151:1–45
37. Weibull W (1951) A statistical distribution function of wide applicability. J Appl Mech 18:293–297
38. Epstein B (1948a) Statistical aspects of fracture problems. J Appl Phys 19:140–147
39. Epstein B (1948b) Application of the theory of extreme values in fracture problems. J Am Stat Assoc 43:403–412
40. Danzer R, Lube T, Supanic P, Damani R (2008) Fracture of ceramics. Adv Eng Mater 10:275–298. https://doi.org/10.1002/adem.200700347
41. Bertalan Z, Shekhawat A, Sethna JP, Zapperi S (2014) Fracture strength: stress concentration, extreme value statistics, and the fate of the Weibull distribution. Phys Rev Appl 2:034008-1–034008-8
42. Todinov MT (2010) The cumulative stress hazard density as an alternative to the Weibull model. Int J Solids Struct 47:3286–3296. https://doi.org/10.1016/j.ijsolstr.2010.08.005
43. Johnson NL, Kotz S, Balakrishnan N (1994) Continuous univariate distributions volume 1, 2nd edn. John Wiley & Sons Inc., New York. https://doi.org/10.1089/gyn.1994.10.129
44. Brown WK, Wohletz KH (1995) Derivation of the Weibull distribution based on physical principles and its connection to the Rosin-Rammler and lognormal distributions. J Appl Phys 78:2758–2763. https://doi.org/10.1063/1.360073
45. Shih TT (1980) An evaluation of the probabilistic approach to brittle design. Eng Fract Mech 13:357–271
46. R'Mili M, Godin N, Lamon J (2012) Flaw strength distribution and statistical parameters for ceramic fibers: the normal distribution. Phys Rev E 85:051106-1–051106-6
47. Reedy ED Jr, Boyce BL, Foulk JW III, Field RV Jr, de Boer MP, Hazra SS (2011) Predicting fracture in micrometer-scale polycrystalline silicon MEMS structures. J Microelectromech Syst 20:922–932. https://doi.org/10.1109/JMEMS.2011.2153824
48. DelRio FW, Friedman LH, Gaither MS, Osborn WA, Cook RF (2013) Decoupling small-scale roughness and long-range features on deep reactive ion etched surfaces. J Appl Phys 114:113506-1–113506-6
49. Gaither MS, DelRio FW, Gates RS, Cook RF (2011) Deformation and fracture of single-crystal silicon theta-like specimens. J Mater Res 26:2575–2589. https://doi.org/10.1557/jmr.2011.319
50. DelRio FW, White RM, Krylyuk S, Davydov AV, Friedman LH, Cook RF (2016) Near-theoretical fracture strengths in native and oxidized silicon nanowires. Nanotechnology 27:31LT02-1–31LT02-7
51. Xu Z, Le J-L (2017) A first passage based model for probabilistic fracture of polycrystalline silicon MEMS structures. J Mech Phys Solids 99:225–241
52. Todinov MT (2009) Is Weibull distribution the correct model for predicting probability of failure initiated by non-interacting flaws? Int J Solids Structures 46:887–901. https://doi.org/10.1016/j.ijsolstr.2008.09.033
53. Zok FW (2017) On weakest link theory and Weibull statistics. J Am Ceram Soc 100:1265–1268. https://doi.org/10.1111/jace.14665
54. Todinov MT (2000) Probability of fracture initiated by defects. Mater Sci Eng A276:39–47
55. Weil NA, Daniel IM (1964) Analysis of fracture probabilities in nonuniformly stressed brittle materials. J Am Ceram Soc 47:268–274. https://doi.org/10.1111/j.1151-2916.1964.tb14413.x